JOURNAL OF SPACECRAFT AND ROCKETS
Vol. 48, No. 3, May–June 2011

Cesium Droplet Evaporation as Contamination Route by Cesium Field Effect Electric Propulsion

T. Tondu,* J.-C. Mateo-Vellez,* and J.-F Roussel†
ONERA, 31055 Toulouse, France
and
E. Chesta‡
Centre National d'Etudes Spatiales, 31401 Toulouse, France

DOI: 10.2514/1.49475

The impact on spacecraft contamination of the emission of cesium droplets by cesium field effect electric propulsion is investigated. This paper focuses mainly on identifying worst-case contamination scenarios, rather than assessing a fully quantitative contamination level. Evaporation of droplets and sputtering mechanisms are compared and the second is shown to be negligible. Cesium droplet evaporation is shown to be self-inhibited by evaporation-induced cooling down. As a consequence, evaporation rate is only controlled by external power deposition on droplets. Evaporation stimulated by solar light absorption and by ion bombardment in the plume are compared and the latter can be neglected, except in the field effect electric propulsion thruster vicinity (a few centimeters). Droplet acceleration by ion beam pressure is considered within the beam, and free transport at constant velocity is considered out of the beam. Contamination levels normalized by the total mass of droplets are estimated in a plane normal to ion beam main direction and containing the thruster. Levels depend on droplet size, initial velocity, and direction of emission (within or out of the beam). Worst-case contamination of, respectively, tens of angstroms, hundreds of angstroms, and thousand angstroms for 1 g of emitted droplets were computed at, respectively, 1 m, 10 cm, and 1 cm from the field effect electric propulsion thruster.

Nomenclature

a	=	acceleration, $\mathrm{m\,s^{-2}}$
C_0	=	droplet material specific heat capacity, $\mathrm{J\,kg^{-1}\,K^{-1}}$
d	=	density, $\mathrm{kg\,m^{-3}}$
dt	=	time step, s
h	=	deposit thickness, m
M	=	molar mass, $\mathrm{kg\,mol^{-1}}$
m	=	mass, kg
m_{Cs}	=	atomic mass, kg
n	=	thruster ion number density, $\mathrm{m^{-3}}$
P	=	power, W
R	=	gas constant: 8.314 $\mathrm{J\,K^{-1}\,mol^{-1}}$
r	=	droplet radius, m
T	=	temperature, K
v	=	velocity, $\mathrm{m\,s^{-1}}$
v_e	=	evaporation rate, $\mathrm{m \cdot s^{-1}}$
α	=	absorbed power fraction
ΔH_{vap}	=	heat of vaporization or sublimation, $\mathrm{J\,mol^{-1}}$
γ	=	surface tension, $\mathrm{J\,m^{-2}}$
ρ	=	distance from field effect electric propulsion, m
Ω	=	solid angle, sr

I. Introduction

SOME very specific spacecraft require low and tunable thrust for acute position control. For instance, thrust requirements for MICROSCOPE (Micro-Satellite à traînée Compensée pour l'Observation du Principe d'Equivalence) and LISA (Laser Interferometer Space Antenna) spacecraft in term of thrust level and thrust noise need the development of never-flown thrust technologies. MICROSCOPE [1] is a satellite by Centre National de la Recherche Scientifique, Centre National d'Etudes Spatiales, and ONERA that will allow (in late 2014) a test of the equivalence principle with a precision of 10^{-15}. For this acute drag, compensation by low thrust is necessary. LISA is a joint NASA–ESA mission to observe astrophysical and cosmological sources of gravitational waves of low frequencies (0.03 mHz to 0.1 Hz, corresponding to oscillation periods of about 10 h to 10 s). The LISA position has to be controlled [2] with an accuracy of 10 nm.

Field effect electric propulsion (FEEP) [3] is a candidate technology considered for such very-low-thrust applications [4]. The propellant is a molten metal that is ionized by field effect. Ions are emitted from the molten metal spike developed under an intense electric field, also called the Taylor cone. Among FEEP thruster technologies considered for MICROSCOPE and LISA, the cesium FEEP developed by Alta [4,5] is based on a slit geometry. Indium FEEP is an alternative technology based on needle geometry.

As for any propulsion, interactions with the spacecraft are considered. For many reasons, cesium is a very unusual and unconventional propellant, but some effects on spacecraft were studied a long time ago [6]. More recent experiments evaluated the effects of cesium contamination on material surface properties [7]. It appeared that because of its low vapor pressure, cesium can reevaporate quite easily from surfaces warmer than −30°C. On the other hand, cesium is a highly electropositive element, and so it is a strong reducing agent. Cesium can react chemically with polymers or some oxides and alter their optical properties.

For estimation of cesium contamination effects, data such as cesium fluxes on spacecraft surfaces must be established. For this, all the relevant contamination routes have to be identified. Collection of charge exchange ions by spacecraft negative surface potentials is one of these routes. This was for instance assessed for MICROSCOPE geometry [8]. Other assessments were performed for indium FEEP, including propellant droplets sputtering [9]. In this paper it is proposed to study how emission of cesium droplets by a cesium FEEP can induce spacecraft contamination. The existence of droplets or clusters emitted by FEEP thrusters or liquid-metal ion sources is well established. Droplet size depends on the ion source operation conditions, but it seems to be generally accepted that the higher the

Received 19 February 2010; revision received 8 September 2010; accepted for publication 26 January 2011.

*Research Engineer, Space Environment Department.
†Head of the Space Environment Department.
‡Electric Propulsion Engineer.

ion current, the bigger the size of droplets [10–12]. With various molten metals, and various field effect ion sources, and various ion currents, droplets cover a wide range of sizes from clusters to tenths of a micrometer [10,11,13]. These droplets are emitted from the tailor cone (or equivalent for a slit geometry) or from the cone edges [13–15]. No droplet formation data are available on the Alta cesium FEEP itself, but this was studied in some conditions on an indium FEEP with needle geometry [12]. Concerning the droplets' angular spread, Czarczynski and Znamirowski [10] indicate that it is much smaller than that of ions, typically 2°. As characteristics of droplets seem to depend on many parameters, we propose in this paper to consider a wide range of sizes from the nanometer to the micrometer.

In this paper the possibility of spacecraft contamination due to droplets emission by a cesium FEEP is investigated. We do not focus on direct contamination by drop collection, but on indirect contamination, where the drops are secondary contamination sources. By contamination we mean a flux of cesium rather that end of life deposit. Indeed, cesium collection can be reversible (by reevaporation) depending on surface materials and temperatures. Several contamination scenarios are investigated and upper contamination flux levels in worst-case conditions are determined. In Sec. II, drops free evaporation is discussed and it is shown that an energy supply is necessary to maintain evaporation. Ion bombardment and sun illumination are two identified possible heating sources and are described in Sec. III. Ion sputtering is another matter emission route that is quantified and compared with evaporation. At last drop charging and transport are qualitatively discussed. More attention is paid on drop acceleration by ion pressure in the plume. At last, on the basis of sun heating a semi quantitative study on spacecraft contamination is estimated for droplets emitted within and out of the ion beam. Focus is given on worst possible contamination levels.

II. Drop Free Evaporation

In this part drop evaporation as a source of spacecraft contamination is studied. The evaporation rate of cesium droplets modeled by perfect spheres of radius r is investigated. Experimental data of cesium evaporation rates on a flat surface are presented elsewhere [7] and are fitted by Eq. (1). Experimental evaporation rate data and fit [leading to Eq. (1)] are presented in Fig. 1. This evaporation rate strongly depends on substrate temperature and follows an Arrhenius law:

$$\frac{dh}{dt} = v_e = -7.210^{15} \cdot \exp\frac{-78,000}{R \cdot T\ (\mathrm{K})} [\dot{A}/\ \mathrm{min}] \tag{1}$$

Evaporation rate for a flat surface can not be directly applied to a droplet geometry because of curvature effects. The dependence on curvature or droplet radius r of evaporation rate is given by the Kelvin Eq. (2) and was applied to cesium using its physical properties presented in Table 1. Figure 2 shows that for droplet radii above a few nanometers, surface tension influence on evaporation rate is low. In this paper it is proposed to neglect surface tension influence and to assume that dh/dt in Eq. (1) is dr/dt for droplet evaporation:

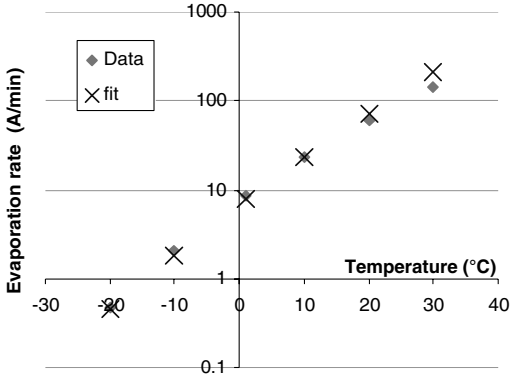

Fig. 1 Cesium evaporation rate.

Table 1 Data for thermal and size evolution study of Cs drops

Data	Value	Unit
Surface tension γ [16]	0.065	$\mathrm{J/m^2}$
Vaporization enthalpy ΔH_{vap}	78,000	J/mol
Molar mass M	133	g/mol
Specific mass heat capacity C_0	240	$\mathrm{J \cdot kg^{-1} \cdot K^{-1}}$

$$\frac{v_e(r)}{v_e(\infty)} = \exp\left(\frac{2\gamma M}{\rho R T r}\right) \tag{2}$$

As evaporation is endothermic, evaporation leads to droplet cooling down and also evaporation rate slowing down. Since evaporation-induced energy loss is proportional to droplet area and heat capacity is proportional to droplet volume, cooling rate due to evaporation follows a r^{-1} law, as presented in Eq. (3) (small droplets cool down more rapidly by evaporation):

$$\frac{dT}{dt} = -\frac{3 \cdot \Delta H_{\mathrm{vap}}}{M \cdot C_0} \cdot \frac{dr}{dt} \cdot \frac{1}{r} \tag{3}$$

On the basis of Eqs. (1) and (3), temperature versus time can be estimated and is presented in Fig. 3 for an initial temperature of 100°C. Main input data are presented in Table 1. The evaporated mass fraction is presented in Fig. 4 and it appears that only a negligible mass fraction evaporates spontaneously in a reasonable time (e.g., 6% of a 10 Å droplet in 1000 s). Indeed, one can assume that 1000 s after being emitted by a FEEP thruster, droplets have

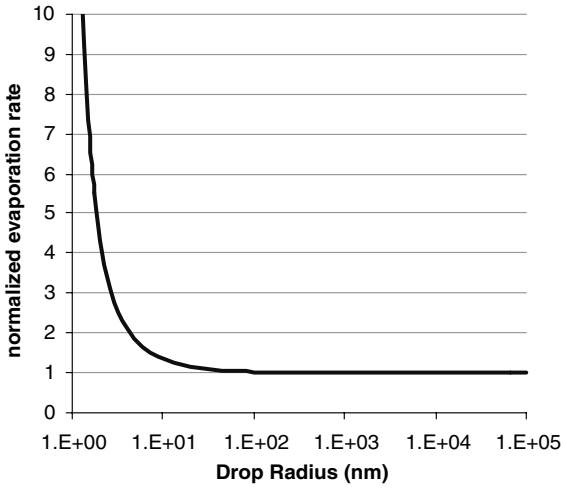

Fig. 2 Influence of drop radius on evaporation rate v_e normalized by evaporation rate of bulk cesium.

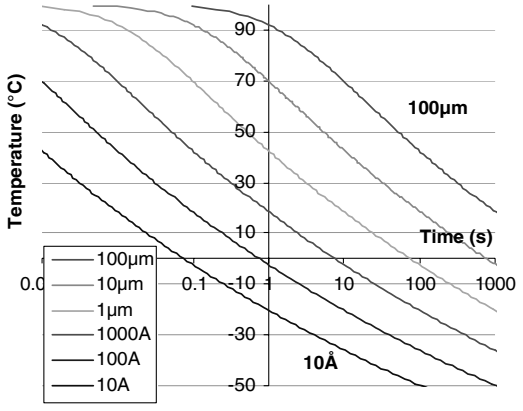

Fig. 3 Spontaneous drop temperature evolutions for initial radii between 100 μm and 10 Å.

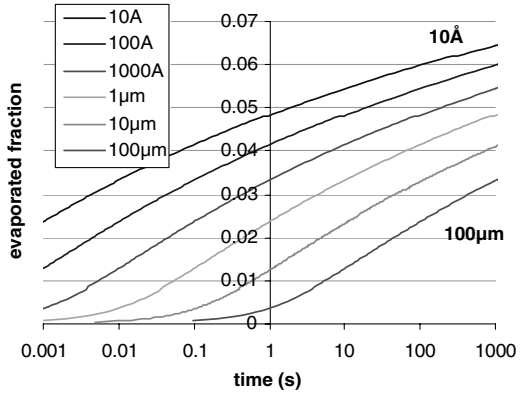

Fig. 4 Time-resolved evaporated mass fraction for an initial temperature of 100°C and for initial radii between 100 μm and 10 Å.

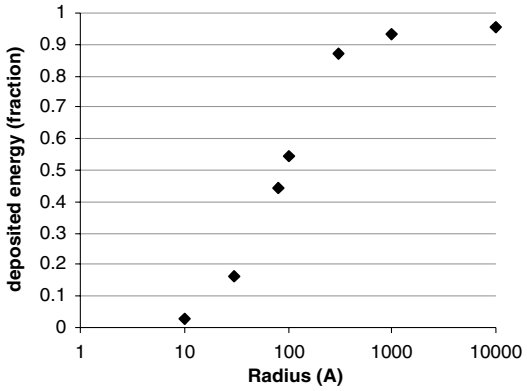

Fig. 5 Estimation of $\alpha(r)$ by CSiPI for 10 keV Cs^+ bombardment.

reached a position too far from the spacecraft to induce severe contamination on it. As a consequence spontaneous evaporation of droplets leading to contamination can be neglected. To be sustained, evaporation-induced cooling down has to be balanced by external energy supply.

III. Drop Stimulated Evaporation

Two sources of external heating are considered for droplet stimulated evaporation: sun illumination absorption and ion-bombardment energy deposition. These two sources can be characterized by their power flux density dP/dS. For solar illumination dP/dS is 1350 W/m^2 in earth vicinity. For ion bombardment by ions generated under the V potential, dP/dS is proportional to ion density n and given is by Eq. (4):

$$\frac{dP}{dS} = n \cdot \sqrt{\frac{2}{m_{\mathrm{Cs}}}} \cdot (qV)^{3/2} \tag{4}$$

This means that sun power density is higher than the ion-bombardment power density when Cs^+ density is lower than 7×10^{12} m^{-3} (for 10 keV ions) that corresponds to few millimeters to centimeters from the FEEP for a typical slit geometry [8]. Obviously this comparison strongly depends on FEEP technology.

In stationary conditions, balance between energy absorption and energy release by evaporation is observed. For example, as cesium evaporation enthalpy is 0.89 eV per atom, a single 10 keV Cs^+ ion absorbed by a droplet can induce evaporation of more than 11,000 Cs atoms. Stimulated evaporation rate can be estimated by Eq. (5), where α is the fraction of the external power flux dP/dS that is absorbed by a droplet. Equation (6) allows establishing the relationship between mass loss rate and radius decrease rate. Equation (7) deduced from Eqs. (5) and (6) indicates that radius decrease rate dr/dt remains constant, whereas heat of vaporization ΔH_{vap} and fraction of absorbed power α are not radius-dependent. As already discussed, curvature effects on evaporation rate can be neglected above few nanometers, and so we consider that ΔH_{vap} is constant. Only $\alpha(r)$ can induce some radius dependence of the radius decrease rate:

$$\frac{dm}{dt} = -\alpha \cdot \frac{dP}{dS} \cdot \pi \cdot r^2 \cdot \frac{M}{\Delta H_{\mathrm{vap}}} \tag{5}$$

$$\frac{dr}{dt} = \frac{dm}{dt} \cdot \frac{1}{d \cdot 4 \cdot \pi \cdot r^2} \tag{6}$$

$$\frac{dr}{dt} = -\alpha \cdot \frac{M}{4 \cdot \Delta H_{\mathrm{vap}} \cdot \rho} \cdot \frac{dP}{dS} \tag{7}$$

For macroscopic objects, the absorbed solar fraction or solar absorptance does not depend on object size. In opposition, for nanodroplets of cesium, it could vary for nanometric sizes because of light transmission possibility and because of surface plasmon absorption. With classical optical laws, transmitted light fraction increases with lower radii because of the lower droplet thickness. With cesium, this effect becomes effective below a few hundreds of nanometers [17]. This lowers the solar absorptance for smaller droplets. In opposition, metallic nanoparticles absorb light specifically when drop size is much lower than light wavelength because of resonance effect with surface plasmons [18]. These size effect are not considered for further calculations and it was assumed that solar light absorption fraction or solar absorptance is not size dependant. A value of 10% is proposed. The impact of this arbitrary choice is discussed later.

In the case of ion bombardment, the fraction of the ion energy deposited in a droplet was estimated using the matter-ion interaction simulation code CSiPI (Code de Simulation de la Pulvérisation Ionique or ONERA Simulation tool for Ion Sputtering) [19]. This code initially devoted to ion sputtering prediction from a flat surface was adapted to droplet geometry. It simulates collision cascades in the target material by a Monte Carlo approach so that energy deposition, sputtering yield, momentum transfer and other information can be generated. All incidences on spherical droplets of different sizes were considered and collision cascades were simulated with droplets of each size. Ion reflections on drops were considered, as well as transmitted ions that only deposit a fraction of their energy. Furthermore, the energy of sputtered atoms was also considered, as this also limits droplet heating.

Figure 5 presents the deposited energy fraction computed using CSiPI for drops bombarded by 10 keV Cs^+ ions. Energy deposition is close to zero for very small particles, because fast ions go through them without deposing much energy. On the contrary, for large droplets, energy deposition reaches a maximum value of 95%. This maximum is reached when ions range in droplets is lower than their size. The missing 5% correspond mostly to reflected ions, and the role of the energy of sputtered atoms is negligible.

IV. Ion Sputtering

Ion sputtering is also identified as a route for droplet mass loss. The sputtering yield prediction code CSiPI [19] was used on droplet geometry in order to estimate sputtering yields for different droplet sizes. As for energy deposition estimation, all incidences were considered. The definition of such a global sputtering yield is not as easy as it seems. The chosen definition is the number of sputtered atoms per ion interacting with the drop. As the atom–ion interaction is a distant interaction, the cylinder that contains the interacting ions is slightly larger than drop section. An alternative definition would have been to consider only a cylinder with same section than the droplet. These two descriptions produce similar results, whereas drop radius is large compared with the ion–atom interaction distance (a few angstroms).

Sputtering yields under 10 keV Cs^+ bombardment predicted by CSiPI are presented in Fig. 6. They range from almost 0 to 90 atoms per ion depending on droplet size. Low sputtering yields correspond

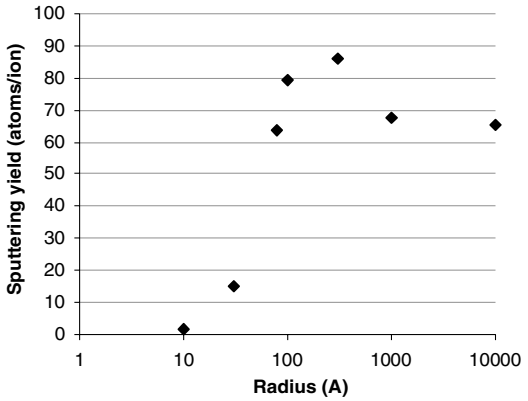

Fig. 6 Droplet sputtering yield estimation under 10 keV Cs^+ bombardment.

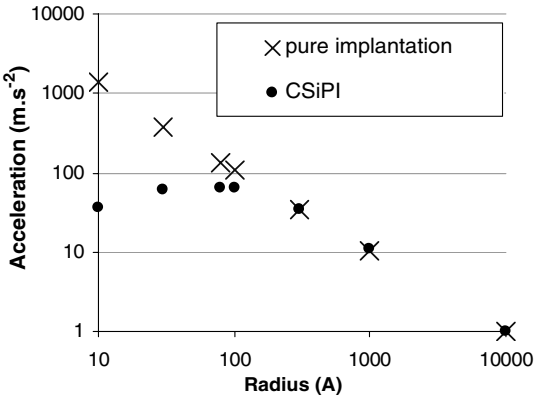

Fig. 7 drop acceleration estimated by simplified analytic formula [Eq. (8)] and by CSiPI for drops in a 10^{12} m^{-3} at 10 keV Cs^+ ions beam.

to low ion energy deposition in droplets. Energy deposition is limited when drop size is smaller than ion range. Maximum sputtering yield is observed when collision cascade size is approximately droplet size. In this case sputtered atoms are emitted downstream and backstream. For larger droplets, only backstream sputtering is possible and the ion sputtering yield becomes constant. This yield is the average sputtering yield of bulk cesium bombarded under various incidences weighted by their probability.

Over the droplet size range of 10 Å to 1 μm, the sputtering yield remains below 90 atoms per ion. This is negligible compared with the previously mentioned 11,000 atoms thermally emitted after 10 keV Cs^+ ion energy absorption. Ion sputtering can be neglected for contamination assessments.

V. Droplet Transport

Droplet transport is obviously a challenging issue for droplet evaporation-induced contamination. Indeed, contamination is proportional to view factors between a surface of interest and a contamination source (a cesium droplet in this case). The view factor is defined as the fraction of solid angle between the source and the studied surface element. Because view factors between an emitted drop and spacecraft surfaces strongly depend on droplet position, no accurate contamination prediction can be performed without solving transport of droplets. It is driven by initial momentum and forces applied to emitted droplets. The main forces applied to cesium droplets are electrostatic force and ion-bombardment pressure in the FEEP plume. In this part, the acceleration due to ion bombardment is quantitatively estimated, whereas charging of droplets and induced effects of electric fields is only qualitatively discussed.

Ion-bombardment pressure results from the transfer of momentum $m_{Cs}.v$ of beam ions to droplets. For an approximated estimation of ion pressure, the following approximations can be proposed:

1) The impinging ions remain implanted inside the drop (total momentum deposition).

2) No sputtering occurs or momentum of sputtered atoms can be neglected.

3) Ion mass is negligible compared with droplet mass.

4) Drop velocity is negligible compared with ion velocity.

These approximations lead to acceleration of droplets impinged by cesium ions of density n and velocity v described by Eq. (8):

$$a = 0.75 \cdot \frac{n \cdot v^2 \cdot m_{Cs}}{d \cdot r} \tag{8}$$

Actually, the above-mentioned approximations are not always verified. More accurate acceleration assessment can be given by the already mentioned CSiPI code adapted to droplets. Figure 7 presents droplet acceleration in a 10^{12} ions/m^2 dense 10 keV Cs^+ plasma for nanometric to micrometric droplets. CSiPI calculations are compared with analytic results obtained using Eq. (8) (total implantation approximation). Above 100 Å in radius, the analytic law is an acceptable approximation. Below 100 Å in radius, Eq. (8) leads to an overestimation of momentum transfer. This result is very similar to energy deposition calculations by CSiPI presented in Fig. 5. For the same reasons only a fraction of ion momentum is transferred to small drops. Nevertheless, momentum transfer efficiency is not directly correlated to energy deposition, because impinging ions that only partly depose their energy are deflected.

For radii above 100 Å, small droplets are more accelerated than large ones. Below 100 Å in radius, acceleration is almost independent of droplet size. As divergence between acceleration under ion pressure calculated by CSiPI and Eq. (8) appears only below 100 Å, it is now proposed to use the latter for velocity calculations of droplets emitted in the ion beam.

With ion pressure, electrostatic force is the second force that can control transport of droplets. Charge is determined by charge collection (ions and electrons) from the plasma and emission (ions, secondary electrons). Note that highly charged drops can split due to coulomb explosion [20]. Charging particles can be Cs^+ ions from the thruster beam, charge exchange ions, neutralization electrons (electric propulsion by positive ions is always neutralized: until now, always by electrons), or local plasma ions and electrons (e.g., ionospheric plasma). Droplets charging and transport are not solved in this paper, but qualitative scenarios are described in the following paragraphs.

Two main localizations can be considered: droplets are either in a neutral plasma or in the extraction electrode electrostatic sheath. In the latter area, the negative bias (typically, 1000 V) of the extraction electrode inhibits electron backstreaming to the positively biased anode so that a whole region is free from electrons. In this area droplet charge is expected to be positive, because it is impinged by fast positive ions. Nevertheless, if droplets are emitted by Taylor-cone cusp detachment it could strongly disturb ions emission and locally stop ion emission. Furthermore, if secondary ion emission under ion bombardment is higher than one, then the drop could get neutralized rapidly by ion bombardment.

Positively charged drops are accelerated then decelerated depending on the electric field (respectively upstream or downstream the extraction electrode). Acceleration and deceleration fields are optimized to focus as much as possible the ion beam. As droplets are very different from ions in term of velocity and charge over mass ratio, it could be expected that emission of charged droplets is much more spread than for ions. Note that because of mass loss (ion-bombardment stimulated evaporation), drops become more and more affected by the field along their path, and so a higher divergence due to deceleration is expected for droplets compared with ions. This qualitative approach indicates that charged droplets could be emitted out of the beam with a given velocity and direction distribution. In opposition, experimental observations tend to indicate that droplet beam is rather focused than spread [10].

In the neutral area (downstream the extraction electrode sheath) two main areas can be considered: droplets in the beam and droplets out of the beam. In the latter case motion of droplets is governed by their charge, the electric field and by the initial velocity vector when they leave the electrostatic sheath. For this study it is considered that

field effect can be neglected. This approximation would need further investigation for validation. In the plume, electric field effect is also neglected, but drop acceleration along the beam by fast ion pressure is considered. Because this acceleration is along the plume, droplets initially in the plume remain within the plume.

VI. Contamination

Contamination is treated as a flux of cesium atoms. Only atoms resulting from droplet stimulated evaporation are estimated in a referential described in Fig. 8. This is a FEEP exit-centered referential, with (Ox, Oy) plane, called FEEP exit plane, set normal to ion beam main direction. Contamination levels in this FEEP exit plane generated by 1 g of droplets were assessed for different emission laws: emission of droplets along the ion beam axis, isotropic emission of droplets, and emission of droplets in a plane parallel to the FEEP exit plane (called *flat emission*). The latter emission law has no physical basis, but is a worst-case configuration.

If the projection of droplet velocity vector along the Oz axis is higher than thermal velocities (a few hundreds of meters/second), no contamination can occur, because velocity vector of evaporated cesium atoms is oriented downstream. In opposition, if it is negligible compared with thermal velocities, it can be considered that evaporated matter emission around a drop in the spacecraft referential is isotropic. It means half downstream, half backstream. Only this second low-drop-velocity case was considered. It was checked that for an initially null droplet velocity, acceleration within the plume by ion pressure leads to maximum velocity increase of a few meters/second. This is negligible compared with thermal velocities.

Contamination on the dS element of the FEEP exit plane (at distance ρ from the FEEP) during the infinitesimal time dt is given by the total evaporation weighted by the solid angle fraction $d\Omega/4\pi$ (view factor). It is interesting to note that for a drop on the Oz axis and for an element dS at distance ρ from the FEEP, the view factor is maximum for $z = \rho$. This means that significant contamination levels at the distance ρ from the FEEP can only be obtained when droplets reach sufficient distances z before total evaporation. For this reason, both high droplet velocities and large droplet diameters favor contamination at high ρ values. In opposition, for high z values, the fraction of evaporated cesium that deposits on the spacecraft is low.

A. Droplets Emitted Along Beam Axis

Droplets emitted within the ion beam are continuously accelerated along the ion velocity vector by ion bombardment, as presented in Fig. 7. Thus, these droplets remain within the plume. Total momentum deposition approximation is considered and drop acceleration is calculated with Eq. (8). As already discussed, cesium droplet evaporation needs to be triggered either by ion-bombardment heating or by solar light absorption. For contamination-level estimations, it is proposed here to neglect ion bombardment compared with sun heating. The consequence of this approximation is that contamination close to the FEEP is underestimated, whereas it is overestimated at higher ρ values. Obviously, this approximation only makes sense when droplets are illuminated. Otherwise droplets are pushed away by ion pressure and induce low contamination levels. We already mentioned the dependence of solar absorptance on droplet size has not been determined. For contamination assessment,

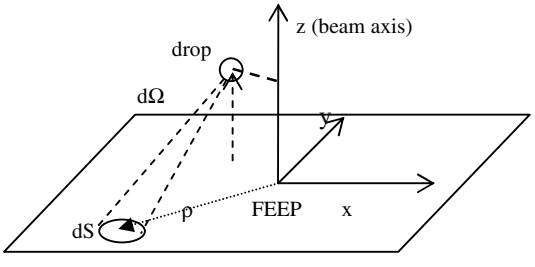

Fig. 8 Reference geometry for contamination study.

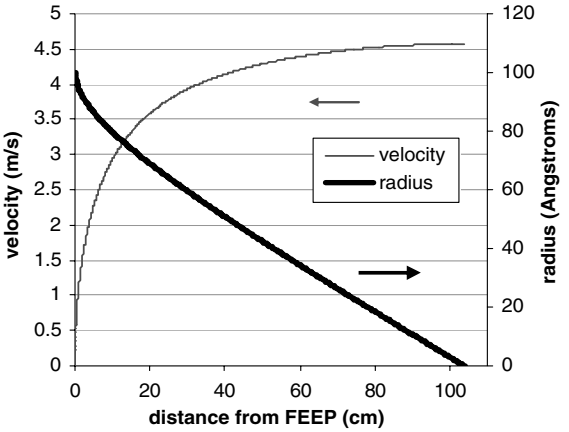

Fig. 9 Drop velocity in the plume.

absorption of 10% of solar irradiance was considered. Using all the above approximations, and assuming an initial null velocity, radius decrease, and velocity increase during drop trip along the Oz axis were calculated. This result is presented in Fig. 9 for an initial radius of 100 Å. The drop is initially rapidly accelerated to a few meters/second and continuously accelerated until it fully evaporates at 100 cm from the FEEP.

Figure 10 presents contamination levels induced by evaporation of 1 g of droplets emitted along the ion beam axis with different initial velocities and for the initial droplet radii 1000 and 100 Å. Close to the FEEP, the lower the initial velocity, the higher the contamination level. At higher ρ values, there can be a worst-case velocity that allows maximum contamination. For instance, 100 Å in radius droplets induce maximum contamination at 100 cm from the FEEP for an initial velocity of 10 m/s. The corresponding contamination level is 50% higher than for null initial velocity. This result is

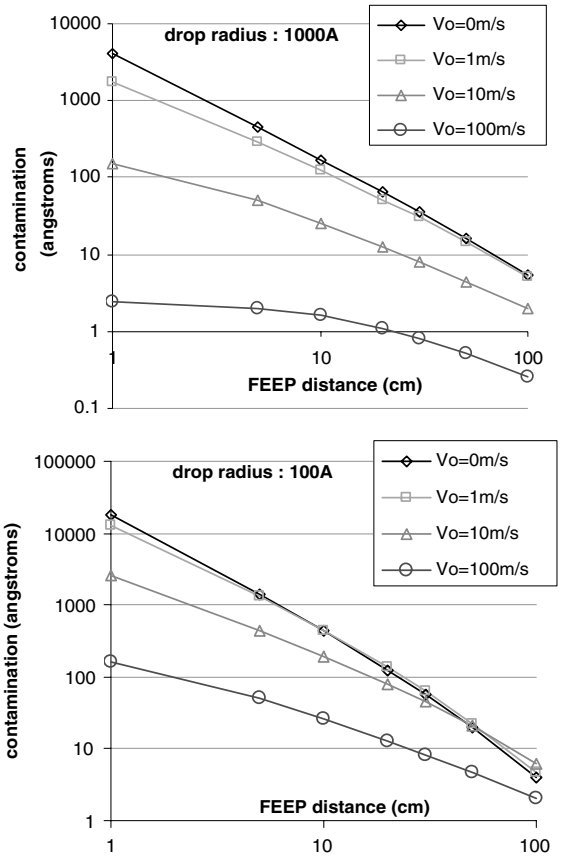

Fig. 10 Influence of initial velocity on contamination levels on FEEP exit plane by 1 g of drop (1000 Å or 100 Å in radius).

explained by the fact that for a given FEEP distance ρ, maximum view factor is obtained when $z = \rho$. Low droplet velocities do not allow reaching such z values, whereas high velocities limit the time spent close to $z = \rho$. Figure 9 indicates that when $z = 100$ cm is reached, droplet size is close to zero, and so induced contamination is negligible.

For droplets of 1000 Å in radius, contamination at 100 cm from the FEEP is maximum for a null initial velocity. The reason for this difference is explained by the fact that such drops reach $z = 100$ cm with a slightly decreased radius. In this condition contamination level is mainly driven by the time spent close to $z = \rho$. As worst-case contamination up to $\rho = 100$ cm is maximum for initial null velocity for 1000 Å and is only 30% below the worst case for 100 Å droplets, only null initial velocity is considered in the next calculations.

Figure 11 presents contamination levels between 1 and 100 cm from the FEEP generated by evaporation of 1 g of droplets emitted along the ion beam axis with initial null velocity. For a given ρ value, there exists a worse droplet size that leads to the highest contamination level. Close to the FEEP, worst droplet size is small, whereas it is large at higher FEEP distance. Between 1 cm and 1 m from the FEEP, this worst size evolves from 30 Å to 300 Å in radius. These radii correspond to typical FEEP thruster droplet sizes. For $\rho = 1$ m, the size of droplets only slightly influence the contamination level induced by evaporation of 1 g of droplets. This contamination level ranges from 3 to 6 Å/g of droplets from 100 Å to 1 μm in radius. Closer to the FEEP, drop size has much more influence. For instance, for $\rho = 10$ cm, contamination levels range approximately from 50 to 500 Å/g of droplets for radii ranging between 100 Å and 1 μm.

The second information given by Fig. 11 is that contamination level decreases rapidly with FEEP distance. Typically, contamination is hundred times lower at 100 cm than at 10 cm from the FEEP. Contamination level given by the worst droplet size can be fitted by a $\rho^{-1.9}$ law.

B. Isotropic Drop Emission

A second investigated droplet emission scenario corresponds to isotropic emission. In this case, acceleration of droplets by beam pressure is neglected, and so straight-line transport at constant velocity is considered. Using Eq. (7), it can be deduced that droplet radius reduction rate dr/dt is constant. For a constant drop velocity v, evaporation ends at the distance ρ_0 given by Eq. (9). For a given $r_0.v$ value, droplets reach a same FEEP exit-centered half-sphere. The quantity of cesium emitted by 1 g of droplets traveling between ρ and $\rho + \delta\rho$ lower than ρ_0, is proportional to the droplet surface (r^2 law) and to radius decay rate (constant). It is inversely proportional to droplet velocity and proportional to the number of droplets ($1/r^3$ law). This means that for any (r_0, v, dr/dt) combination yielding a same ρ_0 value, contamination levels are identical. Note that this is true whatever the chosen emission direction distribution of droplets of constant velocity vector:

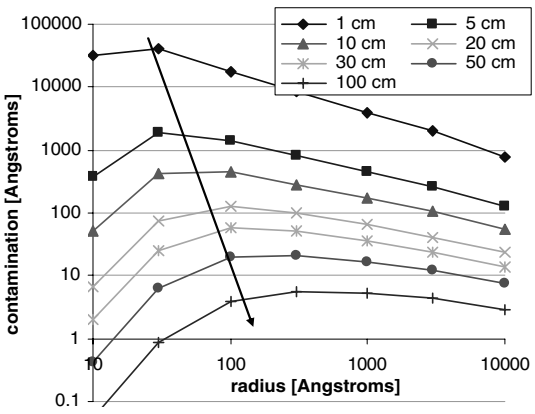

Fig. 11 Contamination by 1 g of drops in the beam as function of their radius for a null initial velocity.

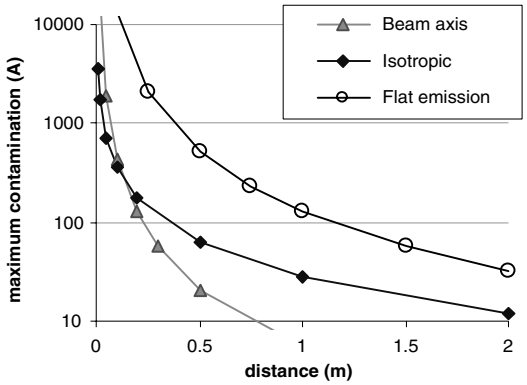

Fig. 12 Maximum contamination on the FEEP exit plane caused by 1 g of droplets for different emission laws.

$$\rho_0 = \frac{r_0 \cdot v}{dr/dt} \tag{9}$$

For each position on the FEEP exit plane, there exists a worse ρ_0 value that induces a maximum contamination level. This means that maximum contamination-level determination does not depend on the chosen solar light absorbed fraction.

For example, for droplets of 1000 Å in radius, maximum contamination at 1 m from the FEEP exit is obtained with a droplet velocity of 1 m/s and solar absorptance of 10%, which is identical to droplet velocity of 0.1 m/s and solar absorptance of 1%. This maximum contamination level induced by evaporation of 1 g of droplets was numerically calculated for any ρ value on the FEEP exit plane. It is plotted in Fig. 12 and compared with the already presented (Sec. VI.A) worst-case contamination level, assuming droplet emission along the ion beam. A third contamination level corresponding to emission in a plane parallel to the FEEP exit plane is also presented. This third emission law, called flat emission, has low physical sense, but is probably the worst-case emission law toward the contamination issue. For flat emission, highest contamination level for a given ρ value is obtained for $\rho_0 = 3\rho$, with worst-case contamination $h_{\max}$ given by Eq. (10):

$$h_{\max} = \frac{m_{\mathrm{Cs}}}{9\pi d} \cdot \frac{1}{\rho^2} \tag{10}$$

The isotropic emission mode leads to contamination levels following approximately a $\rho^{-1.1}$ law. Up to $\rho = 10$ cm droplet emission along beam axis yields the worst-case contamination, whereas for higher ρ values, isotropic emission leads to worst-case contamination levels.

C. Uncertainties

The objective of this study is not to assess contamination levels on a cesium FEEP equipped spacecraft resulting from the existence of emitted cesium droplets. Indeed this has been considered impossible by the authors because of the lack of precise input data for such assessment. The main uncertainties on input data for such a predictive assessment are droplet number, droplet size distribution, droplet emission direction, droplet emission velocity distribution and droplet optical properties.

Furthermore, droplet transport was supposed to be only controlled by an initial velocity and ion pressure acceleration in the thruster plume. No droplet charge effect in the spacecraft electric field was considered. If droplets trajectories are significantly affected by electric fields, they could be focused on negatively biased parts of the spacecraft. This case is not studied here and should be studied.

Depending on the hypothesis, contamination level at a given spacecraft position ranges from no contamination up to the worst-case contamination that has been estimated in this paper. Either the worst case is not problematic for spacecraft mission and the impact of droplets on contamination can be neglected or it is not negligible and further work has to be accomplished to improve the knowledge on input data for an accurate contamination assessment. Emission along

beam axis is the most probable emission law [10], but a fraction of the droplets could also be emitted out of the beam. Figure 12 can be used as a rapid evaluation to identify a potential risk of spacecraft contamination above requirements.

VII. Conclusions

This article shows at least qualitatively that droplet emitted by cesium field effect electric propulsion thrusters can lead indirectly to spacecraft contamination. It has been identified that evaporation of cesium droplets in absence of external heating source is self-inhibited. Two heating sources sustaining evaporation were identified and discussed: ion bombardment and sun illumination (if illuminated), the latter being more important, except in the thruster close vicinity. Solar absorption by droplets has been simplified in this paper and solar absorptance of droplets as a function of their size should be determined for better assessments. At last, it has been shown that ion sputtering of droplets is negligible, compared with heated droplet evaporation.

Worst-case contamination levels in the plane containing the cesium field effect electric propulsion thruster were assessed for 1 g of droplets. This level strongly depends on the chosen emission direction distribution. Emission of droplets in the plume and out of the plume were treated separately, because the first ones are accelerated by ion pressure, whereas the last ones are supposed to move at constant velocity vector. In the latter case it has been shown that for a given emission direction distribution law worst-case contamination at a given distance from the thruster only depends on the length of the trip before total droplet evaporation. As a consequence, hypothesis on drops initial velocity and size and radius decay rate are not necessary. For droplets emitted along the beam axis, the influence of initial velocity and size have been discussed. Droplet size effect is low, except at few centimeters from the thruster exit. Worst-case initial emission velocity is null velocity, except for nanometric droplets.

Considering droplet emission in the plume or isotropic out of the plume, the worst-case contamination levels assessed are, respectively, tens of angstroms, hundreds of angstroms, and thousand angstroms at 1 m, 10 cm, and 1 cm from the field effect electric propulsion thruster. These are no contamination predictions, but upper limits corresponding to worst-case drop size, emission direction, and velocity. Droplets evaporation is shown to be a potential non negligible contamination route compared with collection of charge exchange ions under spacecraft electric fields. Using accurate data on droplets, this work can be used as basis for contamination-level assessment by droplet evaporation.

References

[1] Touboul, P., Rodrigues, M., Métris, G., and Tatry, B., "MICROSCOPE, Testing the Equivalence Principle in Space," *Comptes Rendus de l'Académie des Sciences*, Vol. 2, 2001, pp. 1271–1286. doi:10.1016/S1296-2147(01)01264-1

[2] Ziemer, J. K., and Merkowitz, S. M., "Microthrust Propulsion for the LISA Mission," 40th AIAA/ASME/SAE/ASEE JPC, AIAA Paper 2004-3439, 2004.

[3] Bartoli, C., von Rohden, H., Thompson, S. P., and Blommers, J., "A Liquid Caesium Field Ion Source for Space Propulsion," *Journal of Physics D: Applied Physics*, Vol. 17, 1984, pp. 2472–2483. doi:10.1088/0022-3727/17/12/014

[4] Klotz, H., Strauch, H., Wolfsberger, W., Marcuccio, S., and Speake, C., "Drag-Free, Attitude and Orbit Control for LISA," *ESA/ESTEC 3rd International Symposium on Spacecraft Guidance, Navigation, and Control*, SP-381, ESA, Paris, 1996.

[5] Biagioni, L., Ceccanti, F., Saverdi, M., Saviozzi, M., and Andrenucci, M., "Qualification Status of the FEEP-150 Electric Micropropulsion Subsystem," 41st AIAA/ASME/SAE/ASEE JPC, AIAA Paper 2005-4261, 2005.

[6] Byers, D. C., "Electron Bombardment Thruster Field and Particle Interfaces," *Journal of Spacecraft and Rockets*, Vol. 16, No. 5, Sept.–Oct. 1979, pp. 289–301. doi:10.2514/3.57661

[7] Tondu, T., Chardon, J.-P., Roussel, J.-F., Mateo-Vellez, J.-C., Chesta, E., Tirolien Th., and Perraud, L., "Influence of Spacecraft Contamination by Cesium from FEEPs," Space Propulsion Conference, Paper 2008-42-193, 2008.

[8] Roussel, J. F., Tondu, T., Matéo-Vélez, J-C., Chesta, E., D'Escrivan, S., and Perraud, L., "Modeling of FEEP Plume Effects on MICROSCOPE Spacecraft," *IEEE Transactions on Plasma Science*, Vol. 36, No. 5, Oct. 2008, pp. 2378–2386. doi:10.1109/TPS.2008.2002541

[9] Tajmar, M., Rudenauer, F., and Fehringer, M., "Backflow Contamination of Indium Liquid Metal Ion Emitters (LMIE): Numerical Simulations," International Electric Propulsion Conf., Kitakyushu, Japan, Paper IEPC-99-070, 1999.

[10] Czarczynski, W., and, Znamirowski, Z., "Liquid Metal Ion Sources," *Vacuum*, Vol. 44, Nos. 11–12, 1993, pp. 1095–1099. doi:10.1016/0042-207X(93)90330-D

[11] Thompson, S. P., "Artifacts in High Resolution SIMS: The Contribution of the Ion Source," *Vacuum*, Vol. 34, 1984, pp. 223–228. doi:10.1016/0042-207X(84)90132-5

[12] Tajmar, M., and Genovese, A., "Experimental Evaluation of a Mass-Efficiency Model for an Indium Liquid-Metal Ion Source," *Applied Physics A: Materials Science and Processing*, Vol. 76, 2003, pp. 1003–1006. doi:10.1007/s00339-002-2013-4

[13] Thompson, S. P., and, von Engel, A., "Field Emission of Metal Ions and Microparticles," *Journal of Physics D: Applied Physics*, Vol. 15, 1982, pp. 925–931. doi:10.1088/0022-3727/15/5/021

[14] Forbes, R. G., "Liquid-Metal Ion Sources and Electrosprays Operating in Cone-Jet Mode: Some Theoretical Comparisons and Comments," *Journal of Aerosol Science*, Vol. 31, No. 1, 2000, pp. 97–120. doi:10.1016/S0021-8502(99)00036-1

[15] Forbes, R. G., "Understanding How the Liquid Metal Ion Source Works," *Vacuum*, Vol. 48, No. 1, 1997, pp. 85–97. doi:10.1016/S0042-207X(96)00227-8

[16] Hsu, C. C., and Eyring, H., "Significant Structure Theory of Surface Tension of the Alkali Metals," *Proceedings of the National Academy of Sciences of the United States of America*, Vol. 69, No. 5, May 1972, pp. 1125–1127. doi:10.1073/pnas.69.5.1125

[17] Palik, E. D. (ed.), *Handbook of Optical Constants of Solids*, Vol. 3, Academic Press, New York, 1998, p. 345.

[18] Burchianti1, A., Bogi, A., Marinelli, C., Maibohm, C., Mariotti, E., Sanguinetti, S., and Moi, L., "Optical Characterization and Manipulation of Alkali Metal Nanoparticles in Porous Silica," *European Physical Journal D: Atomic, Molecular and Optical*, Vol. 49, 2008, pp. 201–210. doi:10.1140/epjd/e2008-00164-5

[19] Tondu, T., Viel-Inguimbert, V., Roussel, J. F., and D'Escrivan, S., "Monte Carlo Simulations for HET Ceramics Sputtering Yield Prediction," *Journal of Technical Physics*, Vol. 49, Nos. 3–4, 2008, pp. 363–373.

[20] Tang, K., and Smith, R. D., "Theoretical Prediction of Charged Droplet Evaporation and Fission in Electrospray Ionization," *International Journal of Mass Spectrometry*, Vols. 185–187 1999, pp. 97–105. doi:10.1016/S1387-3806(98)14107-6

D. Edwards
Associate Editor